Article

Influence of Ultrasonic Vibration towards the Microstructure Refinement and Particulate Distribution of AA7150-B4C Nanocomposites

Pagidi Madhukar [1,*], Vipin Mishra [2], Nagamuthu Selvaraj [2], Chilakalapalli Surya Prakasa Rao [3], Veeresh Kumar Gonal Basavaraja [1], Rathlavath Seetharam [4], Murthy Chavali [5,6,*], Faruq Mohammad [7] and Ahmed A. Soleiman [8]

[1] Department of Mechanical Engineering, National Institute of Technology-Andhra Pradesh (NIT-AP), Tadepalligudem 534 101, India; veereshkumargb@nitandhra.ac.in

[2] Department of Mechanical Engineering, National Institute of Technology-Warangal (NIT-W), Warangal 506 004, India; vipinmishra2509@gmail.com (V.M.); selva@nitw.ac.in (N.S.)

[3] National Institute of Technology-Andhra Pradesh (NIT-AP), Tadepalligudem 534 101, India; csp_rao@rediffmail.com

[4] Department of Mechanical Engineering, PDPM Indian Institute of Information Technology, Jabalpur Campus, Khamaria, Jabalpur 482 005, India; seetharam@iiitdmj.ac.in

[5] Office of the Dean (Research) and Division of Chemistry, Department of Science, Faculty of Science & Technology, Alliance University, Chandapura-Anekal Main Road, Bengaluru 562 106, India

[6] NTRC-MCETRC and 109 Nano Composite Technologies Pvt. Ltd., Guntur 522 201, India

[7] Department of Chemistry, College of Science, King Saud University, P.O. Box 2455, Riyadh 11451, Saudi Arabia; fmohammad@ksu.edu.sa

[8] Department of Chemistry, Southern University and A&M College, Baton Rouge, LA 70813, USA; aasoleiman@aol.com

* Correspondence: pmadhu88@gmail.com (P.M.); siva.chavali@alliance.edu.in (M.C.); Tel.: +91-8309-337736 (M.C.)

Abstract: Aluminum-based metal matrix composites with single or multiple ceramic reinforcements are finding application in the aerospace and automobile industries. In this research work, novel AA7150-B4C (aluminium7150 alloy–Boron carbide) nanocomposites were successfully fabricated, through the liquid metallurgy route via stir casting method, with the incorporation of B4C nanoparticles with different weight percentages using a novel sequence of a vortex technique and a double stir casting process with ultrasonication. The formed composites have been thoroughly studied for microstructure refinement, nano-particulate distribution, and bonding with the matrix by making use of the optical microscopy (OM) and scanning electron microscopy (SEM) studies (respectively). In addition, the composites were analyzed for the density, porosity, and elemental composition. Further, the composites were tested for the investigation of mechanical properties, like micro-hardness and tensile strength, to investigate the influence of ultrasonic vibration on the arrangement of B4C nano-particulates. The analysis indicated that the mechanical properties of the AA7150-B4C nanocomposites in as-cast condition significantly improved with a gain of 57.7% in strength and 24.5% in hardness compared to the native AA7150 material.

Keywords: ultrasonic vibration; nanocomposite; boron carbide; AA7150; double stir casting

1. Introduction

Aluminum (Al)-based metal matrix composites (MMCs) are extensively used in automobile, domestic, transportation, and aerospace industries because of their superior thermal conductivity, stiffness, resistance to wear, etc. In general, the Al alloys are available in various series, such as 2xxx, 5xxx, 6xxx, and 7xxx. The 2xxx, 5xxx, and 7xxx alloy series are heat treatable, as they gain their strength from alloying. Prater [1] described that the 7xxx series alloys are the most frequently used materials in aerospace and automobile

applications. Similarly, Li et al. [2] chiefly used an Al-Zn-Cu-Mg composite because of its superior corrosion resistance, as well as strength to weight ratio. In addition, Veeresh Kumar et al. [3], in their investigation, revealed that further improvements in mechanical and tribological characteristics can be obtained by using hard phase ceramic reinforcement particles. Gisele Hammes et al. used hexagonal boron nitride (hBN) as a solid lubricant in Fe-Si-C matrix material to enhance the wear resistance [4]. Several other materials, like graphite [5], silicon carbide (SiC) [6], aluminum oxide (Al_2O_3) [7], etc., are also being used as the reinforcement particles in Al matrices. However, only limited literature on composites reinforced with boron carbide (B_4C) nanoparticles is available, which is due to the high costs and complexions that occur during the fabrication process of these nanoparticles. The B_4C nanoparticles possess attractive properties and are the right choice to use as reinforcement because of their high shock resistance, high melting point and wear resistance, high resistance to a chemical agent, and low specific density (2.52 g/cc).

Mechanical stirring is a conventional and well-known method for the mixing of micro-ceramic reinforcement of particles in molten liquid to produce MMCs. In the case of ultra-fine particles, it is a very challenging task to mix and produce uniform distribution due to the large surface area to volume ratio, which leads to floating on the metal surface and forming the clusters inside the liquid metal. To overcome the floating of nanoparticles, the vortex method has been developed as it produces MMCs in a highly economical way. Additionally, the vortex method helps to avoid the floating of ultra-fine particles on the liquid surface and redirects the particles into the liquid for uniform dispersion. This vortex can be created through a mechanical impeller where the preheated reinforcements are incorporated into the vortex, creating a molten liquid to improve the wetting characteristics among alloy melt and nanoparticles. Two-step stir casting is one of the well-known approaches, which maintains a uniform distribution of ceramic reinforcement of particles in alloy liquid materials. The composite quality can be improved through this technique through a legitimate selection of process parameters, like preheating temperature of ceramic reinforcements, stirring speed, and pouring temperature of the melt. The nanoparticles tend to form high agglomerations and clusters when they are involved with dense liquids. To minimize these problems, Jayakrishnan et al. [8] stated the incorporation of ultrasonic vibrations in molten liquid in their work and analyzed degassing, nanoparticle distribution, and grain refinement properties.

Guo et al. [9] investigated the influence of ball-milled B_4C nanoparticles on Al-B_4C nanocomposite powders and, from the results, the size of matrix powder was found to be decreased with an increase of wt.% of B_4C and milling time. Further, the grain and crystallite sizes were found to be decreased with increased B_4C particle content, along with a transformation to nanograin equiaxed morphology. Alizadeh et al. [10] used the planetary ball milling technique to produce B_4C nanoparticles (20 h) and also fabricated the powders of Al%—4 wt.% B_4C nanocomposite. The mechanical milling processing time was optimized by using density measurements, where the results confirmed that the milling process enhanced the particle content that leads to some fractures and had a hardening effect. It was also confirmed that the uniform distribution of particles influences the hardness of the nanocomposite and the effect of pressure on yield strength through the modified Heckel equation. Jiang et al. [11] fabricated B_4C/BN nanocomposites through the hot-pressing process and chemical deposition, i.e., the B_4C micro-particles were coated with BN nanoparticles through a chemical reaction of $CO(NH_2)_2$ and H_3BO_3 at high temperatures. The investigation was done for the uniform distribution of particles within the composite and grain boundaries. From the results, the fracture toughness and fracture strength of the nanocomposite was found to have decreased with increased content of hBN and also affected the hardness of the nanocomposite significantly. In addition, the formed B_4C/hBN nanocomposite showed excellent machinability at more than 20 wt.% of hBN content. Yaotian Yan et al. [12] developed heterogeneous AgCu alloy material structures with Ti and In reinforcements. the influence of filler materials on the interfacial structure and boundary properties of produced metal joints was observed and the results also revealed

the bonding strength and mechanical performance of the produced heterogeneous metal joint. Chennakesava Reddy [13] analyzed the SiC particle effect on AA6061-SiC composite material, which is fabricated through the stir casting method. From the results obtained, it was noticed that the strength of the composite increased with the content of reinforcement but decreased with an increase of particle size. Qiang et al. [14] manufactured pure Al-SiC composites through ultrasonic vibration (UV)-assisted casting by varying reinforcement volume percentage. The mechanical and microstructural properties were studied at ambient and elevated temperatures.

In Harichandran et al.'s [15] process, high energy ultrasonic waves were introduced to the melt pool to generate a nonlinear effect called transient cavitation and acoustic streaming. Acoustic streaming, as well as the transient cavitation process, involves forming the cavitation bubbles and developing energy levels that are much greater than the energy levels produced by the mechanical stirring process. Therefore, these transient cavitations and macroscopic streaming tend to disperse nanoparticles to prevent agglomeration and enhance the wettability of reinforcement in a molten liquid. From the above discussion, it is also evident that few research works have studied the manufacture of B_4C nanocomposites through the ultrasonic-assisted stir casting process and very limited work has been done to fully characterize it. Therefore, the present work deals with the novel fabrication method to produce uniformly distributed B_4C-reinforced nanocomposites with a sequence of vortex formation, double stir casting, and ultrasonic probe-assisted vibration. It also deals with the study of microstructure and mechanical characterization of AA7150-B_4C nanocomposites.

2. Materials and Methods

Due to its design flexibility, low density, and easy casting, the aluminium7150 alloy (AA7150) was used as a matrix material and the elemental weight percentages were as shown in Table 1. For this, the nano B_4C (boron carbide) was used as a secondary phase reinforcement particle (40–60 nm and >99% purity) to produce the nanocomposite of AA7150-B4C.

Table 1. Chemical composition (%) of AA7150 (Madhukar et al., 2019).

Chemical Composition	Mg	Zn	Cu	Fe	Zr	Si	Mn	Al
AA7150	2.56	6.37	2.25	0.12	0.11	0.08	0.009	Balance (88.501)

Figure 1 shows the schematic diagram of the experimental setup, consisting of an electric resistance heating furnace and an ultrasonication probe. A mechanical stirrer made up of stainless steel (SS 310) with a length of 165 mm and diameter of 65 mm was used to produce the nanocomposites. A thermocouple was used to monitor temperature during the process of melting. An air compressor was used to generate the compressed air and this air was used for cooling and to control the up and down movement of the ultrasonication probe during the sonication process. Argon gas was allowed to pass onto the molten liquid surface to avoid the oxidation of aluminum during the casting process. The AA7150 ingots of 600 g were melted in an arc furnace at 750 °C and choked for an hour. It was stirred mechanically for homogeneous mixing of the melt and then a degassing tablet was used to avoid unwanted gases and K_2TiF_6 was used as a flux to improve the wettability of B_4C nanoparticles.

The B_4C particles were preheated in an electrical furnace (Figure 1b) to avoid moisture content and to improve the wettability of particles to metal liquid. The preheated B_4C nanoparticles were added at many different percentages (0.5%, 1.0%, 1.5%, 2.0 wt.%) to the liquid metal using the vortex method during mechanical stirring and it was performed for 20 min via 2 steps. Each stirring process was 10 min and between the processes, molten metal was allowed to reach a semisolid state. During the mechanical stirring process, the stirrer speed was controlled to maintain the vortex (speed approx. 350–400 rpm). After the two-step stirring process, the ultrasonic probe was dipped (3/4

of liquid) into the melt and allowed to vibrate. In this process, high-energy-intensity waves (frequency of 20 KHz and pulse interval of 10 s) were generated and the produced wave energy was more than that of aluminum liquid bond energy, which breaks the liquid metal bonds to disperse the particles and also creates the micro-cavitation bubbles in a liquid melt. This high-energy cavitation bubble, which was high in pressure (>1000 atm) and high in temperature (5000 °C), broke into clusters and agglomerations due to continuous wave transformation. Therefore, the broken agglomerations spread into the liquid pool. After the ultrasonic vibration process, 5 min of stirring action took place to distribute the broken particles uniformly throughout the melt. The casting liquid was transferred into a preheated die and allowed to cool for the next 24 h. The solidified material blocks were machined as per ASTM standards.
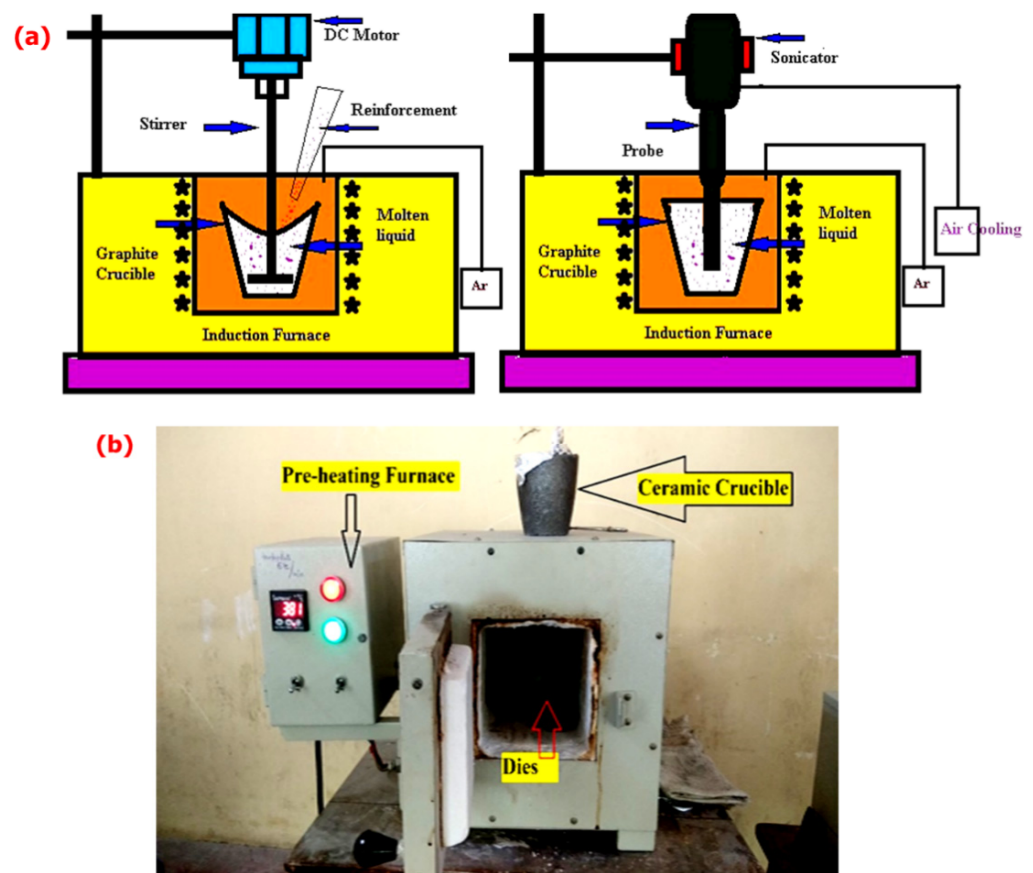

Figure 1. (**a**) Schematic representation of ultrasonic probe-assisted stir casting and (**b**) the preheating chamber used for the formation of AA7150-B4C nanocomposites.

2.1. Sample Preparation

Samples were mirror polished on four different grades of emery paper followed by disc polishing and etching. To study the microstructure analysis through OM/SEM initially, samples were polished manually on I/0, II/0, III/0, and IV/0 silicon carbide emery papers. The direction of polishing changed from one grade to the other. Alternatively, perpendicular directions were selected to eliminate all the hatching lines on the surface of the specimen. Then, the samples were disc polished for 10 min, where aluminum oxide powder was used for the better surface finish while the mirror-like finish was obtained after disc polishing. The polished samples, as shown in Figure 2, were etched with a solution of Kellar etchant, which elevates grain boundaries (25–27 min) on the surface, and the samples were then cleaned with acetone.
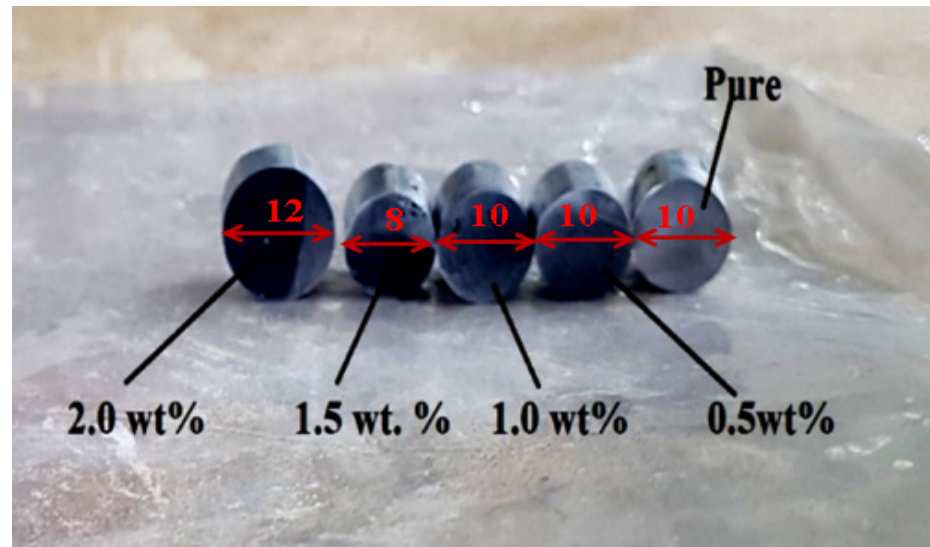
Figure 2. Microstructure samples of AA7150-B4C were prepared (as per 1.5 aspect ratio, dimensions are in mm) with different weight percentages of B_4C.

2.2. Microstructure Study

Optical microscopy (OM) studies were carried out on AA7150-B_4C nanocomposites. The optical microscope (QUASMO, QX-4RT, Haryana, India) uses visible light and a system of lenses to show surface morphology (i.e., the formation of grain distribution) at different magnification views. The microscopic analysis was done for all five samples, (i.e., pure, 0.5, 1.0, 1.5, 2.0 wt.% B_4C-reinforced composite) and the images were taken at different magnification values. Scanning electron microscopy (SEM; Model No.: Vega-3 LMU, Tescan Analytics-Tescan Orsay Holding, Brno-Kohoutovice, Czech Republic) was used to investigate the distribution pattern of particles and the fracture surface. Energy-dispersive spectroscopy (EDS; Model No.: Ultim® Max, Oxford Instruments, High Wycombe, UK) for elemental analysis was carried out.

2.3. Mechanical Properties

The experimental density for various B_4C reinforced nanocomposites was estimated through the Archimedes method. It involves the weight of samples in the air as well as water.

$$\rho = \frac{W_a}{W_a - W_w} \tag{1}$$

where W_a and W_W correspond to the weight of sample in air and water, respectively.

Porosity plays a crucial role in the mechanical behavior of any material; in general, the porosity values will be the norm for the liquid metal process but when the reinforcement material is added to the liquid, the atmospheric air interacts with the ceramic particles and tends to increase the porosity.

$$\text{porosity} = \frac{\rho_{th} - \rho_{ex}}{\rho_{th}} \tag{2}$$

where ρ_{th} is the theoretical density and ρ_{ex} is the experimental density. The ρ_{th} value can be estimated by the rule of mixing equation, as given below:

$$\rho_{th} = \rho_m V_m + \rho_r V_r \tag{3}$$

where ρ_m is the matrix density, V_m is the matrix volume fraction. Similarly, ρ_r and V_r correspond to the density and volume fraction of reinforcement (respectively).

$$V_r = \frac{W_r \rho_m}{\rho_r + W_r(\rho_m - \rho_r)} \tag{4}$$

Here, W_r is the weight percentage of ceramic particles.

Vickers microhardness tester (Model No.: Economet VH 1 MD, Chennai Metco Pvt. Ltd., Chennai, India) was used to test the hardness of B_4C-reinforced nanocomposites, with a 200 g load and 15 s dwell time. Each test was repeated 8 times and the average value was calculated for the best five readings. The tensile test was conducted as per ASTM E8M small (size: 9 mm gauge diameter and 45 mm gauge length) using a universal testing machine (Model No.: WDW-100S, Blue Star Engineering and Electronics Ltd., Mumbai, India). Each test was repeated 3 times and the mean value was calculated.

3. Results and Discussion

3.1. Microstructure Analysis

The yield strength of any material depends on the grain size and the strength increases with respect to the size of grain refinement, as per the Hall–Petch theory. Similarly, the toughness and ductility of a material are significantly affected by the grain size. Throughout the AA7150-B_4C nanocomposite liquid solidification process, the B_4C nanoparticles acted as the center of non-homogeneous nucleation as well as reinforcement of matrix alloy grains. The grain refinement is an attractive mechanism as compared to other strengthening mechanisms and is due to the retention of ductility as well as toughness of the materials.

From Figure 3a–d, it is clear that the formation of grain boundaries increased and grain refinement increased up to 1.5 wt.% with an increase of reinforcement content, and then decreased due to low nanoparticle percolation threshold effect, which leads to a high content of cluster/agglomeration particles along with the nanoparticles [16]. The average grain size (AGS) of each nanocomposite was calculated through the "Linear Intercept Method, AGS = Line of length/No. of grains crossing the line". The length of the line was measured with the help of ImageJ software [17]. The measured values for the average grain size are represented in Figure 3e. Therefore, it was noticed that the percentage of reduction of average grain size at AA7150-1.5% B_4C was 34.68% as compared to 0.5 wt.%. Hence, AA7150-B_4C nanocomposite at 1.5 wt.% had higher strength (180.9 MPa) compared to other weight percentages.
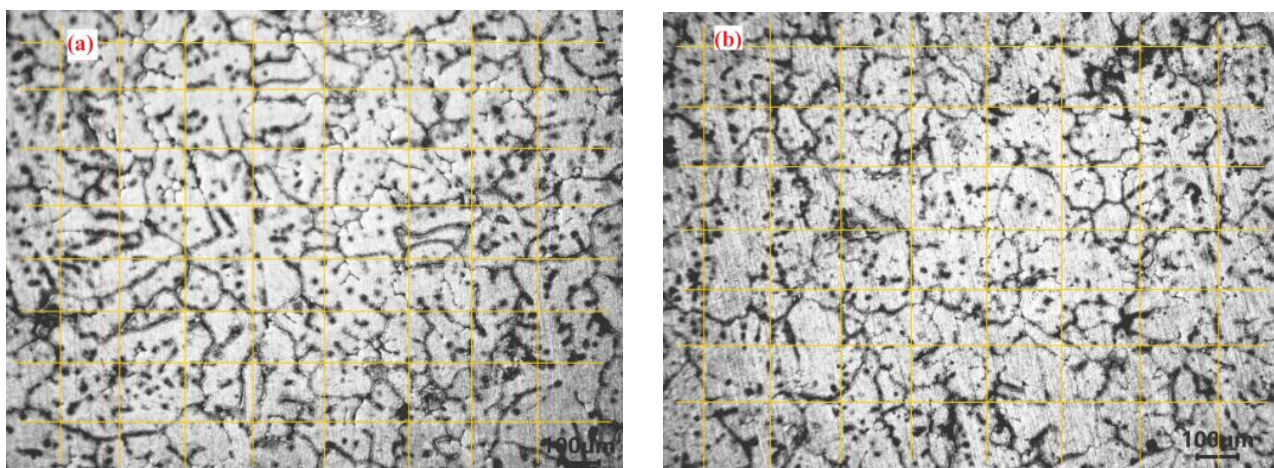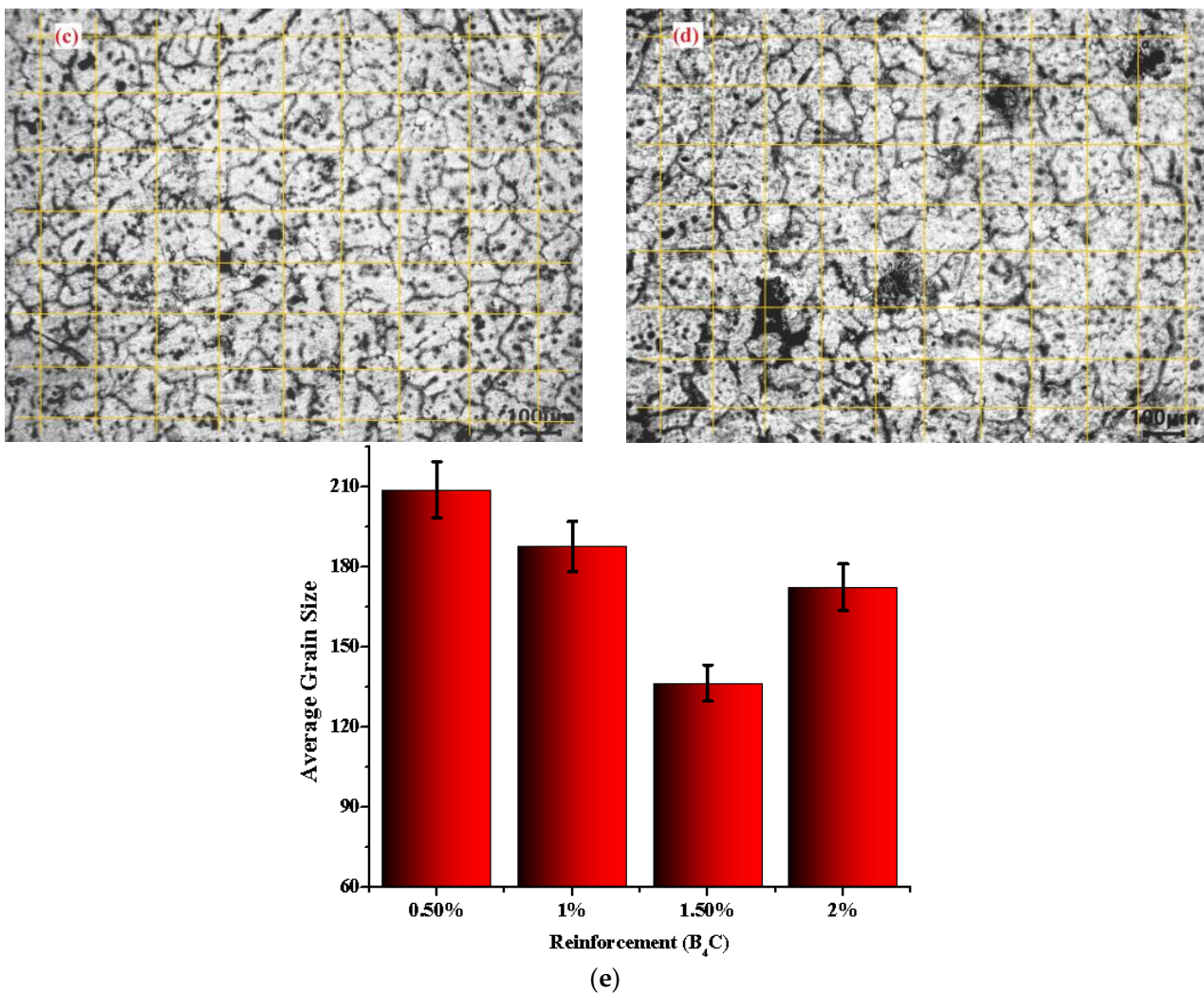

Figure 3. *Cont.*

Figure 3. Optical microscopic images of (**a**) 0.5% B_4C-, (**b**) 1.0% B_4C-, (**c**) 1.5% B_4C-, and (**d**) 2.0% B_4C-reinforced AA7150 nanocomposites, and (**e**) the average grain size.

Figure 4 shows the particle distribution of various weight percentages of nanocomposites by means of SEM analysis and it was noticed that there was a homogeneous distribution of B_4C nanoparticles in the AA7150 matrix in accordance with the wt.% from 0.5, 1.0, 1.5, to 2.0 wt.%. It was also observed that 1.5 wt.% of B_4C represented more particles and enjoyed better homogeneous distribution throughout the nanocomposite as compared to other reinforcements. Figure 4d indicates that the number of voids and cluster formations increased (due to low nanoparticle percolation threshold effect) and the porosity spread around the material, which led to an enhancement in the grain sizes as well as a reduction in the strength of the nanocomposite material. In support of the above statement, the nanoparticles distribution was analyzed through ImageJ software and the number of particles and cluster sizes was observed. From the histogram investigation, the particle size distribution supported the uniform distribution. Figure 4c shows that the higher the number of nano-particulates with uniform distribution, the lower the number of clusters of AA715-1.5 wt.% B_4C composite.

Figure 5 shows the elemental analysis (SEM and EDS) of monolithic and optimal weight percentage of (1.5% B_4C) nanocomposite. It was confirmed with major elements in the monolithic material (pure AA7150), like Al, Cu, Mg, and Zn, and the nanocomposite of AA7150-1.5% B_4C, like Al, Cu, Zn, and Mg, along with reinforced elements, such as B, C. This information supports the idea that the reinforcing of B_4C nanoparticles into

the matrix of AA7150 was successful, and the same conclusion was also verified with XRD analysis.
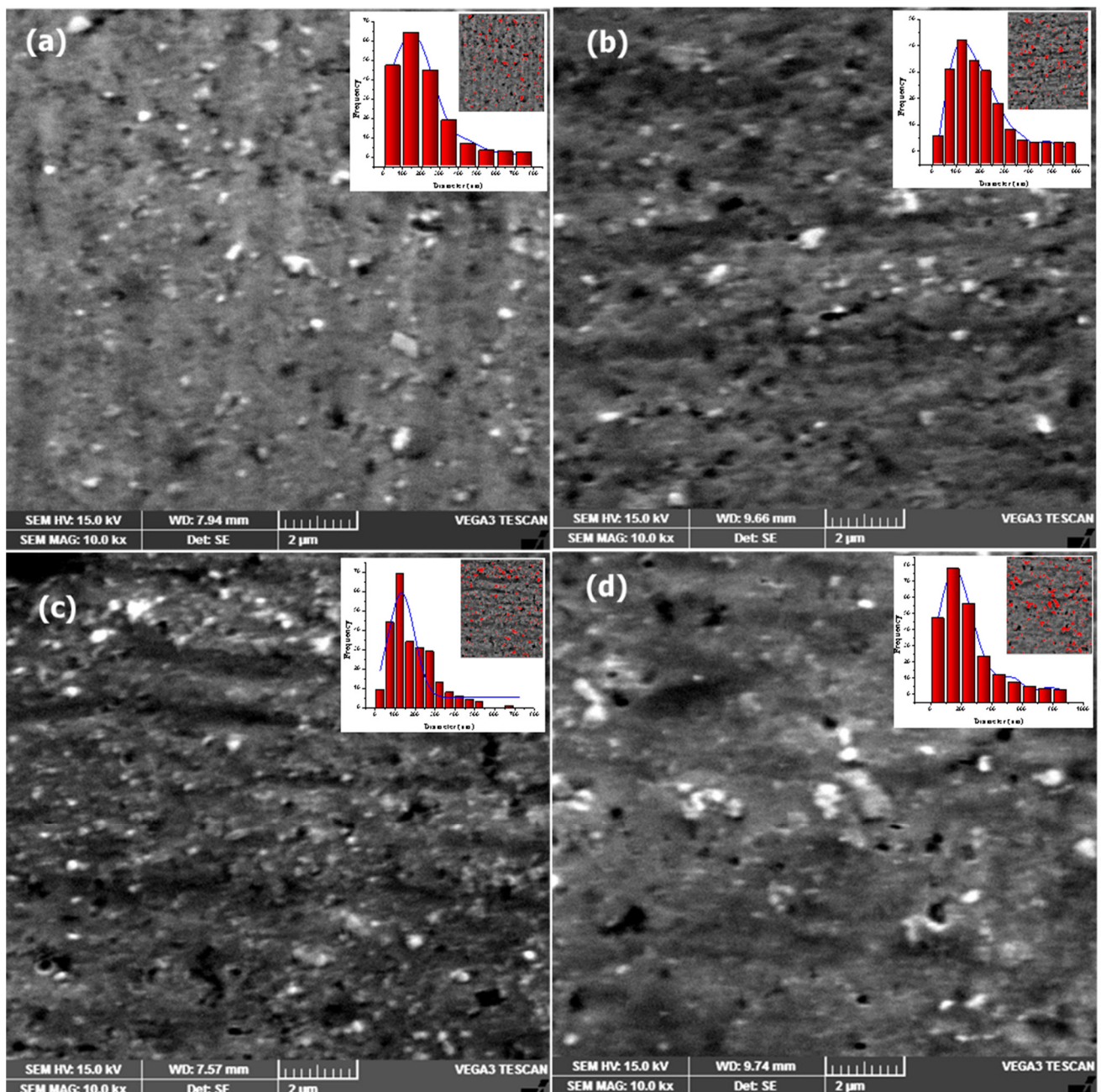

Figure 4. SEM for nanoparticle distribution in the AA7150 matrix with (**a**) 0.5% B_4C, (**b**) 1.0% B_4C, (**c**) 1.5% B_4C, and (**d**) 2.0% B_4C.

3.2. Physical and Mechanical Properties

The theoretical and experimental density of AA7150-B_4C nanocomposites and alloy matrix material was measured by the rule of mixing (Equation (3)) and Archimedes law (Equation (1)), respectively. The porosity involved in AA7150-B_4C nanocomposites and base material was measured by using the porosity equation (Equation (2)), which is based on theoretical and experimental density values.
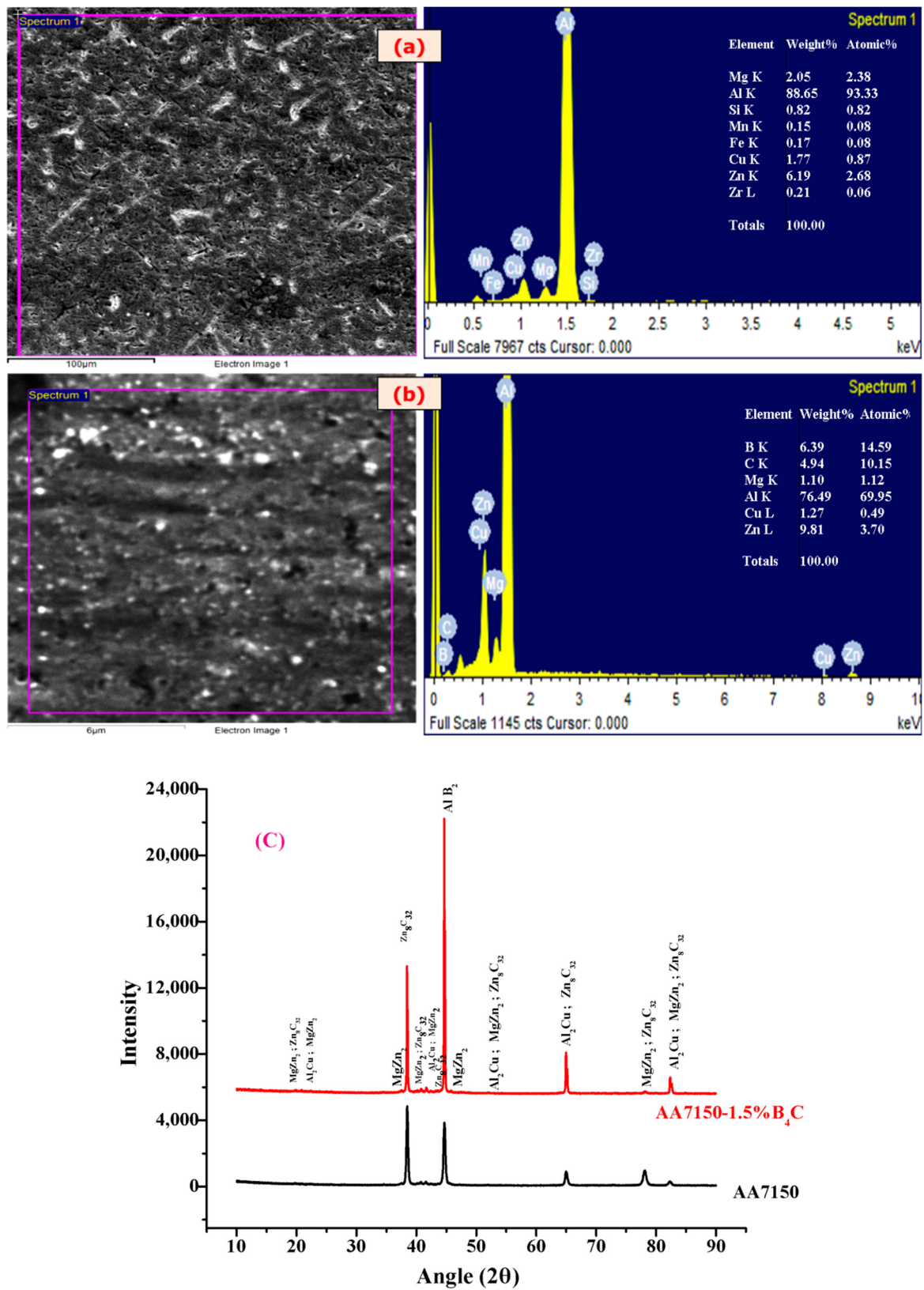
Figure 5. SEM and EDS provided elemental analysis of (**a**) pure AA7150, (**b**) AA7150-1.5% B$_4$C, and (**c**) XRD of AA7150-1.5% B$_4$C nanocomposite.

According to the results obtained, the graphical representation of experimental density and percentage of porosity against wt.% of B_4C nanoparticles is shown in Figure 6a,b (respectively). From the results, it was noticed that the experimental density of AA7150-B_4C nanocomposite decreased with the increase of B_4C nanoparticle content due to lower density of B_4C (2.52 g/cc) particles and the effect of ultrasonic degassing phenomena, which play a vital role in minimizing the porosity. This outcome occurred due to the cavitation effect and closely packed dispersion of B_4C ceramic nanoparticles due to an acoustic streaming effect [18]. In addition, the existence of porosity in AA7150-B_4C nanocomposites and monolithic material was attributed to the theoretical and experimental deference. From the porosity results, it was noticed that the percentage of porosity decreased with an increase of ceramic B_4C nanoparticle content up to 1.5 wt.% and the maximum reduction at 1.5 wt.% of B_4C was due to the degassing effect of ultrasonication and the homogeneous distribution of B_4C nanoparticles throughout the composites as compared to the counterparts [19]. Further, the reinforcement of B_4C nanoparticle content into the AA7150 matrix led to an enhancement in the percentage of porosity and this was due to the large surface area to volume ratio of ceramic nanoparticles, voids, and the cluster formation [20].
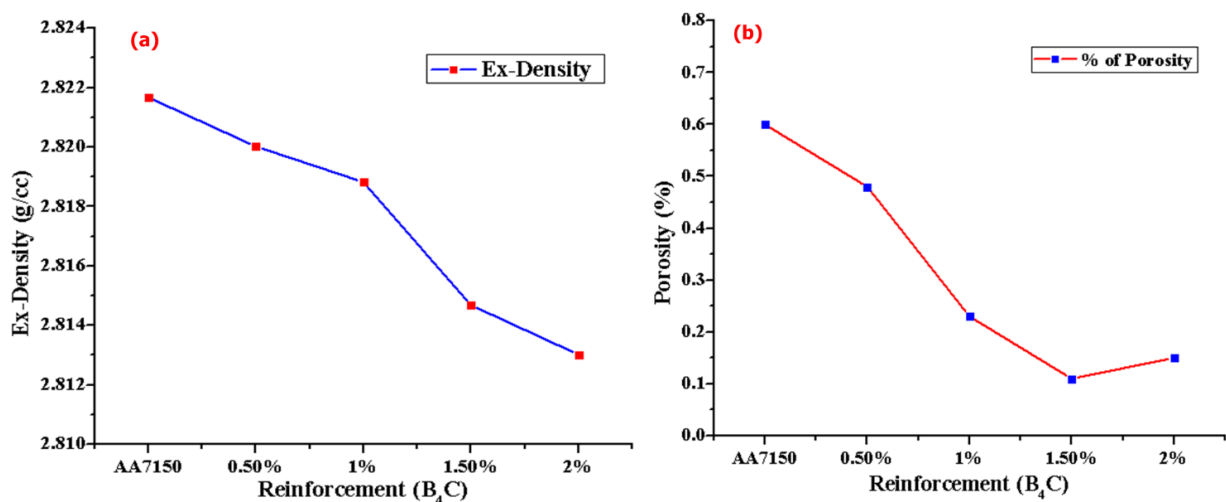

Figure 6. (**a**) Density and (**b**) porosity measurements against B_4C reinforcement.

Figure 7 shows the results of the Vickers hardness test for various nanocomposites of AA7150-B_4C, where the microhardness behavior is represented through a bar graph. From the graph, it can be seen that the microhardness of B_4C nanoparticle-reinforced AA7150 matrices increased positively with increased B_4C nanoparticle weight percentage up to 1.5% due to harder B_4C ceramic particles, which strengthened the composite material [21,22]. This kind of observation can also be linked to a better interaction between the AA7150 matrix and the reinforced B_4C nanoparticles, Hall–Petch (grain refinement), and Orowan strengthening mechanism (uniform distribution of ceramic nanoparticles due to ultrasonication effect), which restricted the deformation during the indentation [23].
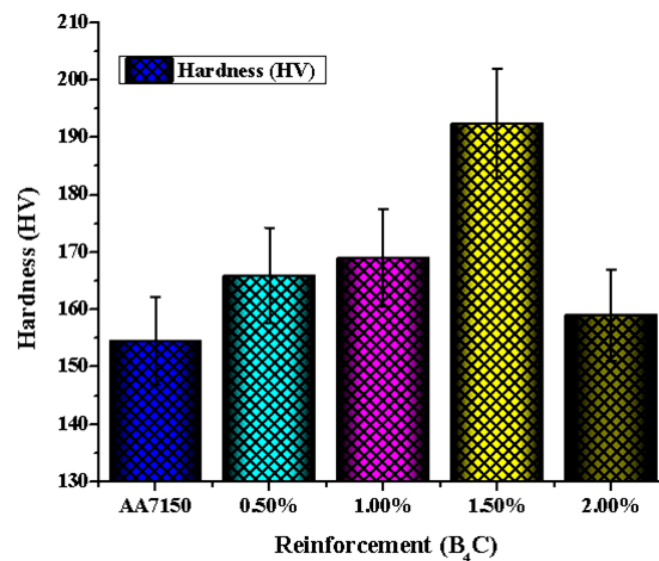
Figure 7. Comparison of datasets for micro-hardness vs. wt.% B$_4$C for the base AA7150 matrix before and after reinforcing B$_4$C (with different wt.%).

Similarly, Figure 8a shows the tensile properties of the base AA7150 compared with that of AA7150-B$_4$C nanoparticles (with different wt.%) at room temperature and the corresponding stress–strain curves are shown in Figure 8b. The effect of B$_4$C reinforcement in AA7150 nanocomposites was analyzed for the tensile values and it was observed that the ultimate strength increased positively with B$_4$C nanoparticles up to 1.5 wt.% due to the nanoparticle load-bearing effect, as well as the coefficient of thermal expansion (CTE) mismatch strengthening mechanism. The CTE variation of AA7150 ($23.2 \times 10^{-6}/°C$) and B$_4$C nanoparticles ($5 \times 10^{-6}/°C$) influenced the results due to thermally developed residual stress and high dislocation density, which acts as a barrier to the movement of dislocation in the nanocomposite material [24]. This result can also be rightly attributed to the homogeneous distribution of ultra-fine B$_4$C ceramic particles in the nanocomposites and to the ultrasonic probe-assisted vibration in the aluminum melt bath, leading to the homogeneous distribution of nanoparticles and grain refinement during the solidification process. This phenomenon promotes the enhancement of tensile strength in the nanocomposite material as compared to the pure alloy matrix [25]. Hence, the AA7150-B$_4$C nanocomposite strength increased with B$_4$C nanoparticle content up to 1.5 wt.% (the values of ultimate tensile strength for base metal and 1.5 wt.% of B$_4$C nanoparticle-reinforced nanocomposites were 114.7 MPa and 180.9 MPa) and then decreased further. This decrement of ultimate strength in AA7150-2 wt.% B$_4$C was mainly due to clusters/agglomerations and microvoids, which promote the stress concentration in the nanocomposites [26]. In addition, the micro-hardness and ultimate tensile strength significantly improved by 154.5–192.4 HV (57.7%) and 114.7–180.9 MPa (24.5%) and were found to have optimal properties at 1.5%B$_4$C.

3.3. Fracture Surface

Tensile fracture surface fractographic images at $100\times$ magnification for the base metal and different weight percentages of B$_4$C reinforcement are shown in Figure 9. Figure 9a–e reveals that the number of cracks, voids, and grape-shaped dendrites globules acted as a stress riser and led to a crack [27]. These moderately increased with an increased weight percentage of reinforcement particle content. Figure 9d confirms that the voids and cracks were minimized as compared to other weight percentages. Further increment in weight percentages led to an increase in huge voids and cracks of various shapes and sizes, as confirmed by Figure 9e. It also confirmed that the facets and dimples were present. Therefore, the nature of the failure of AA7150-B$_4$C is a mixed kind of partially brittle and ductile mode [28].
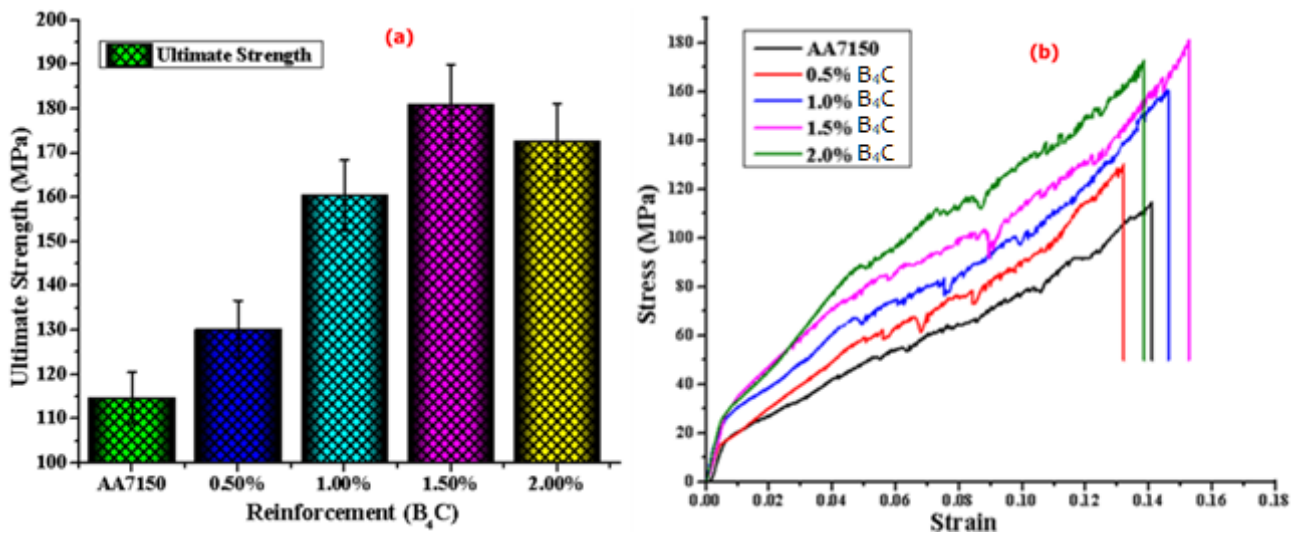
Figure 8. Comparison of (**a**) ultimate strength Vs wt.% B$_4$C and (**b**) stress–strain data for monolithic and AA7150-B4C nanocomposites.
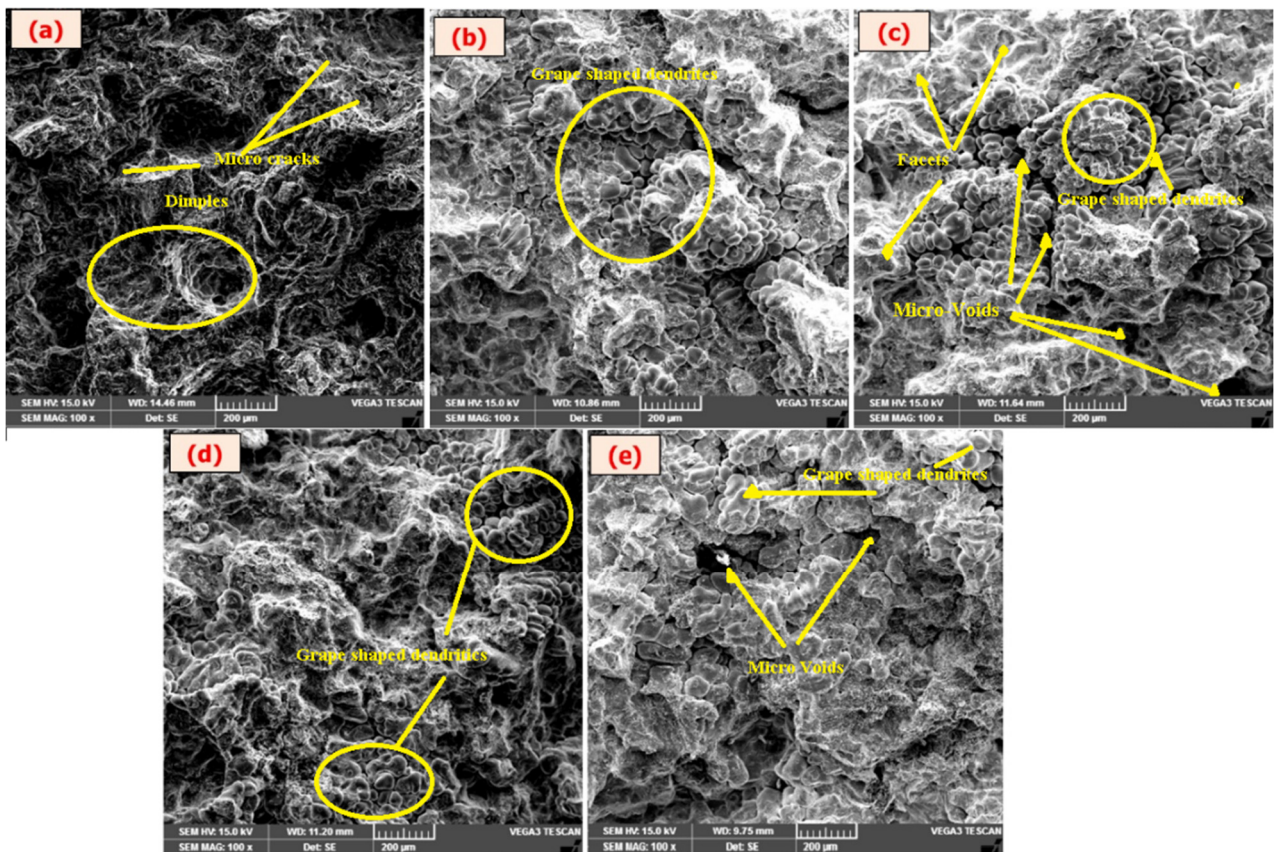

Figure 9. Fractured surfaces of (**a**) Al7150 alloy, and (**b**) 0.5% B$_4$C-, (**c**) 1.0% B$_4$C-, (**d**) 1.5% B$_4$C, and (**e**) 2.0% B$_4$C-reinforced AA7150 matrices.

The optimal weight percentage fractography was enlarged for the fracture surface analysis and it is represented in Figure 10, showing the enlarged image of 1.5% B$_4$C nanocomposite at 20 μm from a 200 μm fractography. The enlarged photography shows many stepwise dendrites and facets. At the same time, it is also revealing that the B$_4$C strength of the next crystal layer, which elevated the high surface energy and friction

between adjacent interfaces, required detaching the particles. Therefore, it led to the optimal strength of nanocomposites.
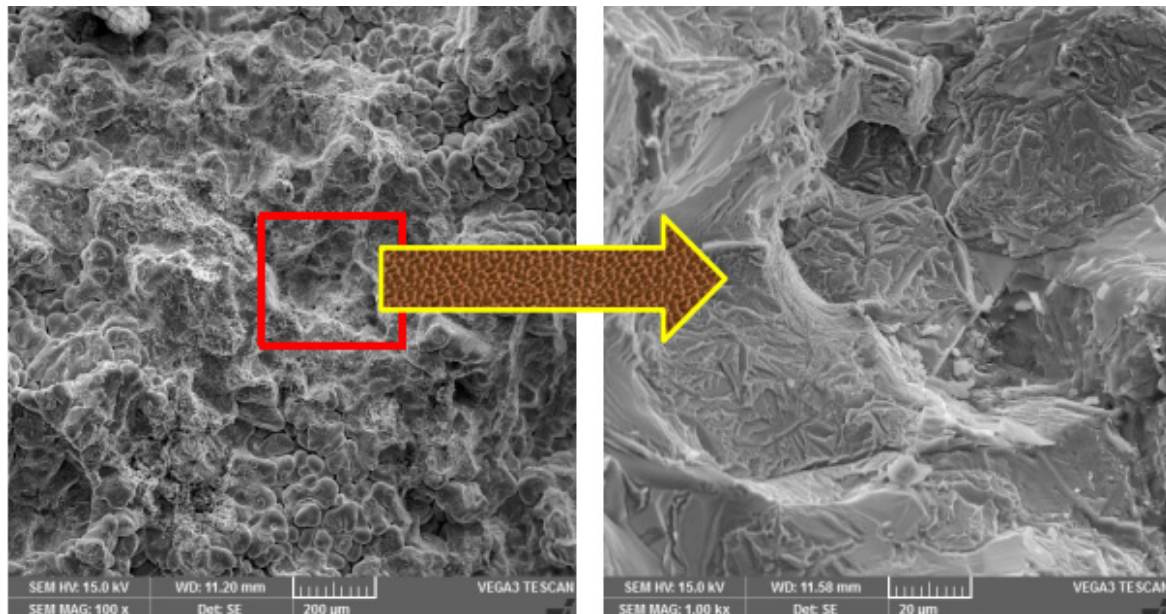

Figure 10. The enlarged fracture surface of the 1.5% B_4C nanocomposite.

4. Conclusions

In the present study, the AA7150-B_4C nanocomposites were successfully manufactured through an ultrasonic vibration-assisted double stir casting process using the vortex method. The experiments were conducted in the as-cast condition. On testing of the composite, the mechanical properties were found to be increased with an increase of B_4C particle reinforcement of up to 1.5% wt. and further increments led to a reduction in properties due to the presence of voids and clusters. In addition, the microstructure analysis confirmed the ultrasonic vibration formation of good grain boundaries, grain refinement, and uniform distribution of nanoparticulates at 1.5% B_4C as compared to other percentages. The measurement of porosity indicated that the porosity values decreased with an increase of B_4C nanoparticle content and we observed a minimum of 1.5% B_4C (0.11%). The micro-hardness and ultimate tensile strength significantly improved by 154.5–192.4 HV (57.7%) and 114.7–180.9 MPa (24.5%) and were found to have optimal properties at 1.5% B_4C. The fine ductility of AA7150-B_4C was maintained without compromising its strength and a maximum ductility of 16.27% was reported at an optimal weight percentage of B_4C. The fractographic studies revealed the brittle nature of failure in nanocomposites.

Author Contributions: Conceptualization, M.C.; Data curation, P.M. and C.S.P.R.; Formal analysis, P.M., V.M., N.S., C.S.P.R., V.K.G.B., R.S., M.C., F.M. and A.A.S.; Funding acquisition, F.M.; Investigation, P.M.; Methodology, P.M. and V.K.G.B.; Resources, V.M., N.S., C.S.P.R., R.S., F.M. and A.A.S.; Supervision, M.C.; Validation, R.S.; Writing–review & editing, M.C. All authors have read and agreed to the published version of the manuscript.

Institutional Review Board Statement: Not applicable.

Informed Consent Statement: Not applicable.

Data Availability Statement: The data presented in this study are available on request from the corresponding author.

Conflicts of Interest: The authors declare no conflict of interest.

References

1. Prater, T. Friction Stir Welding of Metal Matrix Composites for use in aerospace structures. *Acta Astronaut.* **2014**, *93*, 366–373. [CrossRef]
2. Li, J.F.; Jia, Z.Q.; Li, C.X.; Birbilis, N.; Cai, C. Exfoliation corrosion of 7150 Al alloy with various tempers and its electrochemical impedance spectroscopy in EXCO solution. *Mater. Corros.* **2009**, *60*, 407–414. [CrossRef]
3. Kumar, G.B.V.; Rao, C.S.P.; Selvaraj, N. Mechanical and Tribological Behavior of Particulate Reinforced Aluminum Metal Matrix Composites—A review. *J. Miner. Mater. Charact. Eng.* **2011**, *10*, 59–91. [CrossRef]
4. Hammes, G.; Mucelin, K.J.; Gonçalves, P.D.C.; Binder, C.; Binder, R.; Janssen, R.; Klein, A.N.; de Mello, J.D.B. Effect of hexagonal boron nitride and graphite on mechanical and scuffing resistance of self lubricating iron based composite. *Wear* **2017**, *376–377*, 1084–1090. [CrossRef]
5. Ilija, B.; Jovana, R.; Biljana, B.; Miroslav, B.; Aleksandar, V.; Slobodan, M. Microstructural characterization and artificial aging of compo-casted hybrid A356/SiCp/Grp composites with graphite macroparticles. *Mater. Sci. Eng. A* **2014**, *612*, 7–15.
6. Cao, G.; Konishi, H.; Li, X. Mechanical Properties and Microstructure of Mg/SiC Nanocomposites Fabricated by Ultrasonic Cavitation Based Nanomanufacturing. *J. Manuf. Sci. Eng.* **2008**, *130*, 031105. [CrossRef]
7. Morteza, A.; Hossein, A.B. Strength prediction of the ARBed Al/ Al2O3/B4C nanocomposites using the Orowan model. *Mater. Res. Bull.* **2014**, *59*, 290–294.
8. Nampoothiri, J.; Harini, R.S.; Nayak, S.K.; Raj, B.; Ravi, K. Post in-situ reaction ultrasonic treatment for generation of Al–4.4Cu/TiB2 nanocomposite: A route to enhance the strength of metal matrix nanocomposites. *J. Alloys Compd.* **2016**, *683*, 370–378. [CrossRef]
9. Guo, H.; Zhao, Y.; Xu, S.; Li, J.; Liu, N.; Zhang, Y.; Zhang, Z. Influence of high B4C contents on structural evolution of Al-B4C nanocomposite powders produced by high energy ball milling. *Ceram. Int.* **2019**, *45*, 5436–5447. [CrossRef]
10. Alizadeh, A.; Taheri-Nassaj, E.; Baharvandi, H.R. Preparation and investigation of Al–4 wt% B4C nanocomposite powders using mechanical milling. *Bull. Mater. Sci.* **2011**, *34*, 1039–1048. [CrossRef]
11. Jiang, T.; Jin, Z.; Yang, J.; Qiao, G. Investigation on the preparation and machinability of the B4C/BN nanocomposites by the hot-pressing process. *J. Mater. Process. Technol.* **2009**, *209*, 561–571. [CrossRef]
12. Yan, Y.; Liu, T.; Lin, J.; Qiao, L.; Tu, J.; Qin, S.; Cao, J.; Qi, J. Interaction between the third alloying element and the interfacial structure of AgCu-alloy brazed heterogeneous metal integration. *J. Alloys Compd.* **2021**, *883*, 160933. [CrossRef]
13. Reddy, A.C. Influence of Particle Size, Precipitates, Particle Cracking, Porosity and Clustering of Particles on Tensile Strength of 6061/SiCp Metal Matrix Composites and Validation Using FEA. *J. Mater. Sci. Manuf. Eng.* **2015**, *42*, 1176–1186.
14. Li, Q.; Qiu, F.; Dong, B.X.; Geng, R.; Lv, M.M.; Zhao, Q.L.; Jiang, Q.C. Fabrication, microstructure refinement and strengthening mechanisms of nanosized SiCP/Al composites assisted ultrasonic vibration. *Mater. Sci. Eng. A* **2018**, *735*, 310–317. [CrossRef]
15. Harichandran, R.; Selvakumar, N. Effect of nano/micro B4C particles on the mechanical properties of aluminium metal matrix composites fabricated by ultrasonic cavitation-assisted solidification process. *Arch. Civ. Mech. Eng.* **2016**, *16*, 147–158. [CrossRef]
16. Xuan, Y.; Nastac, L. 2018. The role of ultrasonic cavitation in refining the microstructure of aluminium-based nanocomposites during the solidification process. *Ultrasonics* **2018**, *83*, 94–102. [CrossRef]
17. Jiang, D.; Yu, J. Fabrication of Al2O3/SiC/Al Hybrid Nanocomposites Through Solidification Process for Improved Mechanical Properties. *Metals* **2018**, *8*, 572. [CrossRef]
18. Isfahani, M.J.N.; Payami, F.; Asadabad, M.A.; Shokri, A.A. Investigation of the effect of boron carbide nanoparticles on the structural, electrical and mechanical properties of Al-B4C nanocomposites. *J. Alloys Compd.* **2019**, *797*, 1348–1358. [CrossRef]
19. Liu, X.; Zhang, C.; Zhang, Z.; Xue, J.; Le, Q. The role of ultrasound in hydrogen removal and microstructure refinement by ultrasonic argon degassing process. *Ultrason. Sonochem.* **2017**, *38*, 455–462. [CrossRef]
20. Madhukar, P.; Rao, C.S.P.; Selvaraj, N. Manufacturing of aluminium nanohybrid composites: A state of review. *Mater. Sci. Eng.* **2016**, *149*, 12114.
21. Khodabakhshi, F.; Gerlich, A.P.; Worswick, M. Fabrication and characterization of a high strength ultra-fine grained metal-matrix AA8006-B4C layered nanocomposite by a novel accumulative fold-forging (AFF) process. *Mater. Des.* **2018**, *157*, 211–226. [CrossRef]
22. Bahrami, A.; Soltani, N.; Pech-Canul, M.I.; Soltani, S.; González, L.A.; Gutiérrez, C.A.; Tapp, J.; Möller, A.; Gurlo, A. Bilayer graded Al/B4C/rice husk ash composite: Wettability behavior, thermo-mechanical, and electrical properties. *J. Compos. Mater.* **2018**, *52*, 3745–3758. [CrossRef]
23. Hosseini, N.; Karimzadeh, F.; Abbasi, M.H.; Enayati, M.H. Tribological properties of Al6061–Al2O3 nanocomposite prepared by milling and hot pressing. *Mater. Des.* **2010**, *31*, 4777–4785. [CrossRef]
24. Wang, X.J.; Wang, N.Z.; Wang, L.Y.; Hu, X.S.; Wu, K.; Wang, Y.Q.; Huang, Y.D. Processing, microstructure and mechanical properties of micro-SiC particles reinforced magnesium matrix composites fabricated by stir casting assisted by ultrasonic treatment processing. *Mater. Des.* **2014**, *57*, 638–645. [CrossRef]

25. Madhukar, P.; Selvaraj, N.; Gujjala, R.; Rao, C.S.P. Production of high performance AA7150-1% SiC nanocomposite by novel fabrication process of ultrasonication assisted stir casting. *Ultrason. Sonochem.* **2019**, *58*, 104665. [CrossRef] [PubMed]
26. Su, H.; Gao, W.; Feng, Z.; Lu, Z. Processing, microstructure and tensile properties of nano-sized Al2O3 particle reinforced aluminium matrix composites. *Mater. Des.* **2012**, *36*, 590–596. [CrossRef]
27. Bembalge, O.B.; Panigrahi, S.K. Development and strengthening mechanisms of bulk ultrafine-grained AA6063/SiC composite sheets with varying reinforcement sizes ranging from nano to microdomain. *J. Alloys Compd.* **2018**, *766*, 355–372. [CrossRef]
28. Maleque, M.A.; Adebisi, A.A.; Izzati, N. Analysis of Fracture Mechanism for Al-Mg/SiCp Composite Materials. *Mater. Sci. Eng.* **2017**, *184*, 012031. [CrossRef]